CrossMark

ORIGINAL PAPER

Carboxymethyl cellulose/poly(acrylic acid) interpenetrating polymer network hydrogels as multifunctional adsorbents

Paulo V. O. Toledo · Diego P. C. Limeira · Nicolas C. Siqueira · Denise F. S. Petri

Abstract Interpenetrating polymer network (IPN) hydrogels were prepared by mixing carboxymethyl cellulose (CMC) solution and crosslinked poly(acrylic acid) (cPAA) single IPN hydrogel at mass ratios 100:0, 25:75, 50:50, 75:25 and 0:100 and subsequent crosslinking of CMC chains with citric acid, aimed towards the creation of full IPN hydrogels. The resulting CMC:cPAA hydrogels were freeze-dried for the determination of density, swelling degree, compressive modulus and thermal behavior. Morphological and structural parameters were determined by means of scanning electron microscopy, Fourier transform infrared spectroscopy in the attenuated total reflectance mode (FTIR-ATR) and X-ray microtomography (CT) analyses. The efficiency of CMC:cPAA hydrogels as adsorbents for methylene blue (MB) dye at pH 7 and Cu^{2+} ions at pH 4.5 was systematically investigated at (24 ± 1) °C and evaluated with Langmuir, Freundlich and Dubinin–Radushkevitch adsorption models and kinetic equations. The CMC:cPAA 50:50 hydrogels were particularly interesting because they presented the highest compression modulus $(141 \pm 3$ kPa), swelling degree of 58 ± 2 g_{water}/g and maximum adsorption capacity (q_{max}) for MB dye and Cu^{2+} ions as 613 mg g^{-1} and 250 mg g^{-1}, respectively. The adsorption kinetics of MB and Cu^{2+} ions followed the pseudo-second order equation. Fitting with the intraparticle diffusion model showed that in both cases, the adsorbate molecules first diffuse rapidly from the medium to the adsorbent surface, and then in a second slower stage, they diffuse into the network macropores. The hydrogels could be recycled five times without losing efficiency.

Keywords Carboxymethyl cellulose · Interpenetrating polymer networks · Hydrogels · Adsorption · Methylene blue · Copper ions

P. V. O. Toledo · D. P. C. Limeira · N. C. Siqueira · D. F. S. Petri (✉)
Institute of Chemistry, University of São Paulo, Av. Prof. Lineu Prestes 748, São Paulo 05508-000, Brazil
e-mail: dfsp@iq.usp.br

Introduction

Polysaccharide-based adsorbents for analyte pre-concentration or removal of pollutants are particularly interesting because they can carry different adsorbing sites, and they stem from renewable sources (Crini 2005). Carboxymethyl cellulose (CMC) is a water soluble cellulose ether, which behaves as polyanion at pH > 4.5, widely used in pharmaceutical, cosmetic and food formulations due to its nontoxicity and

biocompatibility (Heinze and Koschella 2005; Thielking and Schmidt 2012). The ability of CMC chains to form hydrogels aimed towards the removal of dyes and metal ions stimulated the development of interesting adsorbents. CMC and hydroxyethyl cellulose (HEC) crosslinked with fumaric acid led to hydrogels with swelling degrees (SD) that decreased as the cation valence increased (Seki et al. 2014). The addition of CMC isolated from pineapple peel to gelatin and alginate hydrogels improved the swelling, ionic and electric behavior (Dai et al. 2017). CMC coated magnetic particles were successfully applied for the removal of dye (Zirak et al. 2017) and trivalent lanthanide Eu(III) (Cai et al. 2017). The increase in the CMC degree of substitution led to CMC coated polystyrene particles with more negative zeta potential values and higher adsorption capacity for Cu^{2+} ions (Soares et al. 2005). Crosslinking of CMC with further grafting dimethyldiallylammonium led to particles able to adsorb anionic and cationic dyes (Lin et al. 2016). Membranes of CMC-graft-poly(acrylic acid) (PAA) synthesized in the presence of silica gel led to efficient adsorbents for Cd(II) ions and crystal violet dye (Saber-Samandari et al. 2016). Composites of CMC-g-PAA and attapulgite, a natural clay, exhibited excellent adsorption properties for Pb(II) (Liu et al. 2010).

Hydrogels can be classified as physical and chemical networks swollen by water. In the physical hydrogels, the polysaccharide chains are held together in a 3D network by molecular entanglements, electrostatic interactions, H bonding or van der Waals interactions. Changes in temperature, pressure, ionic strength, or shear can disrupt the intermolecular forces and the 3D structure. In the chemical hydrogels, the chains are linked by crosslinkers, making them more stable than the physical hydrogels (Dragan 2014). However, in order to achieve high performance in terms of mechanical and swelling properties, interpenetrating polymer network (IPN) hydrogels are more indicated. IPNs combine distinct coexisting networks. In a full IPN both components are present as cross-linked networks, although there is negligible bonding between the two polymers, whereas in a semi-IPN, only one polymer is present as a network. (Roland 2013).

Semi-IPNs involving CMC and PAA have been applied to improve the swelling properties (Bajpai and Mishra 2004; Wang et al. 2011) and for drug release (Bajpai and Mishra 2005); in both cases the acrylic acid monomer was polymerized and crosslinked in the presence of CMC physical network. In this work, full IPNs hydrogels were prepared by mixing a crosslinked PAA single IPN hydrogel (cPAA or Carbomer 940^{TM}), widely applied in the formulation of cosmetics and topical antiseptic gels, with CMC at different compositions and subsequent crosslinking of CMC chains with citric acid, a nontoxic crosslinker, aimed towards the creation of full IPNs hydrogels. To the best of our knowledge, the simple crosslinking of CMC chains by citric acid in a commercial single IPN is a new strategy for the preparation of full IPNs. The resulting CMC:cPAA hydrogels were freeze-dried and characterized. The characterization of freeze-dried hydrogels, also called cryogels (Smirnova and Gurikov 2017), comprised the determination of density, degree of swelling, compressive modulus and thermal behavior. Structural analyses were performed by scanning electron microscopy (SEM), Fourier transform infrared spectroscopy in the attenuated total reflectance mode (FTIR-ATR) and X-ray microtomography (CT) analyses. The efficiency of CMC:cPAA hydrogels as adsorbents for Cu^{2+} ions and methylene blue (MB) dye from aqueous media was systematically investigated and evaluated with Langmuir, Freundlich and Dubinin–Radushkevitch (D–R) adsorption models and kinetic equations. The possibility of hydrogels recycling was also investigated. MB and copper ions were chosen as adsorbates because they can be found as pollutants in natural waters.

Materials and Methods

Materials

Carboxymethyl cellulose (CMC, 419338 Sigma-Aldrich, DS 0.9, M_v 4.210^5 g mol^{-1}, determined by capillary viscometry Supplementary Material SM1), crosslinked poly(acrylic acid) (cPAA, Carbomer 940 V001385 Sigma-Aldrich), citric acid (Labsynth, Brazil, 192.12 g mol^{-1}), cyclohexane (Labsynth, Brazil, 84.16 g mol^{-1}), sodium hypophosphite (HPS, Labsynth, Brazil, 105.99 g/mol), methylene blue (MB, M9140 Sigma-Aldrich, 319.85 g mol^{-1}), Trizma Base (Tris, Sigma-Aldrich, 121.14 g mol^{-1}), and cupric sulfate pentahydrate (Labsynth, Brazil,

249.69 g mol^{-1}) were used as received. Since Carbomer 940 is composed of PAA chains already crosslinked with erythritol, it does not dissolve in water or other solvents, making the determination of its molecular weight by conventional methods (capillary viscometry, dynamic light scattering, etc.) very difficult.

Hydrogel preparation

Figure 1 shows schematically the preparation of hydrogels. Aqueous solutions of CMC or aqueous dispersions of cPAA were prepared in MilliQ water at 2.0 wt%, containing 0.10 wt% citric acid and 0.05 wt% HPS, as crosslinker and catalyst, respectively. Citric acid and HPS were also added in the cPAA in order to avoid dilution upon mixing with CMC solutions. The dispersion of cPAA in water turned the medium acid (pH $\sim$ 4). Upon neutralization with some droplets of NaOH 1.0 mol L^{-1} the opaque dispersion became a clear gel. After that, CMC solution and PAA gel were mixed at five different compositions CMC:cPAA 0:100, 25:75, 50:50, 75:25 and 100:0, which were used as precursors for the cryogels.

The mixtures of CMC:cPAA were poured into acrylic cylindrical molds of 10 mm diameter and 6 mm high. The samples were frozen for 2 h in a standard freezer at $-$ 24 °C, followed by 8 h of freeze-drying under vacuum (0.02 mbar). The cooling rate is an important parameter because it affects the nucleation and size of ice crystals (Deville 2013). In order to get insight about this parameter, thermocouples were embedded in the middle of the cylindrical molds containing the mixtures and the temperature

was measured as a function of time. The cooling curves presented typically three regions: (1) linear decrease of temperature from 27 °C to $-$ 0.5 °C, at $\sim$ 2.0 °C min^{-1}, (2) an isothermal phase transition plateau at $-$ 0.5 °C and (3) cooling from $\sim$ $-$ 0.5 to $\sim$ $-$ 24 °C, as shown in the Supplementary Material SM2. Similar cooling curve was observed for MilliQ water. All polymer solutions were frozen under the same conditions. However, some of them presented supercooling effects, which could not be correlated to any particular experimental condition.

The freeze-dried hydrogels, or cryogels, were withdrawn from the molds and heated for 7 min at 165 °C to promote the esterification between citric acid and hydroxyl groups from CMC chains. This procedure has been successfully applied for the crosslinking of CMC (Li et al. 2008), hydroxypropyl methylcellulose (Marani et al. 2015; Martins et al. 2017; Souza and Petri 2018) and xanthan (Bueno et al. 2013; Bueno and Petri 2014) chains. In order to evaluate the effect of citric acid on the crosslinking of CMC chains, a set of CMC:cPAA samples were prepared in the absence of citric acid and HPS, afterwards they were heated for 7 min at 165 °C.

Characterization of freeze-dried hydrogels

In order to evaluate the content of crosslinked CMC chains (gel content), the dried cryogels were weighed and immersed in MilliQ water for 48 h with periodic change of water. The water was changed until the conductivity no longer changed. After that, they were freeze-dried and weighed again. This procedure was also done for a set of CMC:cPAA samples prepared in the absence of citric acid.
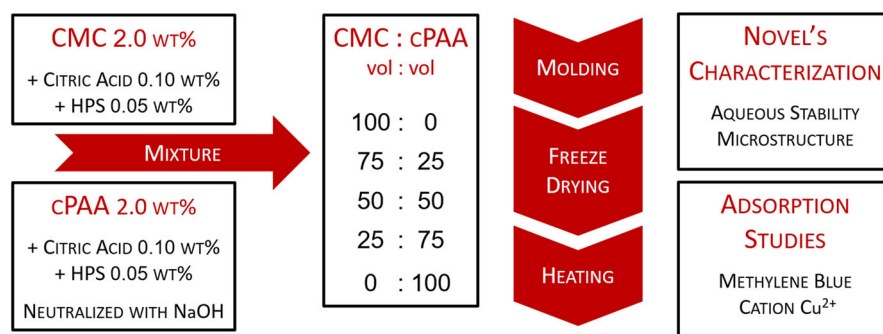
Fig. 1 Schematic representation of hydrogels and cryogels preparation for further characterization and adsorption studies

Gel content was calculated according to Eq. 1:

$$Gel(\%) = \left[1 - \left(\frac{m_{pol} - m_{dried}}{m_{pol}} \right) \right] \times 100 \qquad (1)$$

where m_{pol} is the initial mass of polymer (cPAA and/or CMC) and m_{dried} is the mass of freeze dried sample.

For the characterization, the hydrogels were rinsed with MilliQ water until the rinsing water achieved conductivity of $\sim$ 5 µS/cm. This procedure removed the unreacted molecules, which could be only physically attached to the hydrogels. After that, they were freeze-dried and weighed again.

The swelling degree (SD) was determined with a precision tensiometer Krüss K100 at 22 ± 1 °C as the mass of sorbed MilliQ water (pH 5.5) at equilibrium (m_{water}) divided by the mass of dried adsorbent, which was on average 13 ± 1 mg:

$$SD = \frac{m_{water}}{m_{dried}} \qquad (2)$$

SD values were also determined in 0.010 mol L^{-1} HCl (pH 2.0), 0.0001 mol L^{-1} NaOH (pH 10.0). The effect of ionic strength on SD was evaluated at pH 5.5, 0.010 mol L^{-1} or 0.100 mol L^{-1} NaCl.

The apparent density (ρ_{ap}) of dried cryogels was determined by weighing them in an analytical balance and measuring their dimensions with a pachometer over ten samples, at 22 ± 1 °C and relative air humidity of $60 \pm 10\%$. Thermogravimetric analyses (TGA) were performed with a thermobalance ISI sTA i1500, in the temperature range from 25 to 950 °C, under dynamic N_2 atmosphere (50 mL min^{-1}), at heating rate of 5 °C min^{-1}. Fourier transform infrared vibrational spectra in the attenuated total reflectance mode (FTIR-ATR) were obtained with a Perkin Elmer Frontier with Zn/Se crystal equipment with resolution of 4 cm^{-1}, in the range of 600–4000 cm^{-1}; the spectra are the average of 50 individual scans. Compression tests were performed with a digital dynamometer IP 90DI-10 with a load cell of 10.0 N, limit of applied force of 0.1 N and accuracy of 0.5%, at 22 ± 1 °C and air relative humidity of $60 \pm 10\%$. Scanning electron microscopy (SEM) analyses were conducted with a JEOL Neoscope JCM 5000 equipment, operating at voltage of 10 kV, on samples coated by sputtering with 5 nm of gold. X-ray microtomography (CT) analyses were performed with a Skyscan 1272 Bruker equipment, operating at 20 kV and 175 uA. The sample was rotated stepwise (0.6° per step) through

360°, and images were recorded at each step with an exposure time of 5 s, yielding spatial resolution of 10 µm. On average, 600 X-ray images were taken in 60 min, scanning along the whole sample, yielding images with spatial resolution of 10 µm. The thresholding of calculated gray scale images (from 13 to 255) and the transformation of the CT data into microstructural parameters were performed for all samples in the same way, using the CTAn Bruker software.

Adsorption studies

All dried adsorbents used for the adsorption studies were cylindrical samples 6 mm high and 10 mm diameter (Supplementary Material SM3). The adsorption studies were conducted in aqueous media. Upon immersion in water, the crosslinked cryogels became swollen, behaving as IPNs hydrogels. For the adsorption studies, methylene blue (MB) and copper ions (Cu^{2+}) were chosen. Prior to the adsorption studies, the hydrogels were rinsed with MilliQ water until the rinsing water achieved conductivity of $\sim$ 5 µS/cm. This procedure removed the unreacted molecules, which could be only physically attached to the hydrogels. After that, they were freeze-dried and weighed again. For all adsorption studies the mean mass of dried adsorbent (m) amounted to 20 ± 2 mg and the volume of adsorbate solution was 5 mL.

MB solutions were prepared in Tris–HCl buffer, at pH 7.0, in order to avoid adsorption on the glass vials and self-assembling. The affinity of MB for the CMC:cPAA hydrogels was investigated in batch and kinetics adsorption experiments at 24 ± 1 °C. For the batch adsorption experiments, the dried adsorbents were immersed in MB solution at the concentration values of 1.6, 3.1, 4.7, 6.3, 7.8, 9.4, 11.0 and 12.5 µmol L^{-1} (or 0.5, 1.0, 1.5, 2.0, 2.5, 3.0, 3.5 and 4.0 mg L^{-1}), for 24 h under constant rotation at 5 rpm in a homemade vertical carrousel. The adsorption kinetics was investigated for MB solutions at 1.6 and 12.5 µmol L^{-1}. The MB concentration in the supernatant was measured after 30 min, 1 h, 2 h, 4 h, 6 h and 24 h contact.

Batch and kinetics adsorption experiments of Cu^{2+} ions on hydrogels were performed at 24 ± 1 °C. The solutions of $CuSO_4 \cdot 5H_2O$ were prepared in the concentration range of 5.0 g L^{-1} (0.02 mol L^{-1}) to 50 g L^{-1} (0.20 mol L^{-1}), at pH 4.5, in order to avoid

precipitation of $Cu(OH)_2$. At pH smaller than 3.5 the adsorption practically did not take place, probably due to the protonation of carboxylate groups. For the batch adsorption experiments, the dried adsorbents were immersed in Cu^{2+} solutions prepared at the concentration values of 0.04, 0.06, 0.08, 0.10 and 0.20 mol L^{-1} (or 10, 15, 20, 25.0 and 50.0 g L^{-1}), in the concentration range of 10.0–50.0 g L^{-1}, for 2 h, under constant rotation at 5 rpm in a homemade vertical carrousel. The adsorption kinetics was investigated for Cu^{2+} solutions at 12.5 g L^{-1} and 37.5 g L^{-1}. The concentration of Cu^{2+} ions in the supernatant was measured after 2, 4, 6, 10, 15, 30, 45, 60, 75, 90 and 120 min contact.

The concentration of free MB molecules or Cu^{2+} ions in the supernatants was determined by UV–Vis spectrophotometry at 662 nm and 700 nm, respectively, in a Beckman-Coulter DU640 spectrophotometer. The corresponding calibration curves are available as Supplementary Material SM4. The concentration of adsorbed MB molecules or Cu^{2+} ions onto the hydrogels was determined as the difference between the initial concentration (C_0) and the concentration in the supernatants, or the equilibrium concentration (C_e). The equilibrium adsorption capacity (q_e, mg g^{-1}) was calculated dividing the concentration of adsorbed specie by the mass of dried adsorbent (m) and multiplying by the solution volume (v):

$$q_e = \frac{C_0 - C_e}{m} \times v \tag{3}$$

The mean q_e values correspond to the average of at least duplicates. All experimental data were processed with OriginPro9 software.

Hydrogel recycling

In order to evaluate the possibility for hydrogels recycling, dried hydrogels (mean mass 20 ± 2 mg) were inserted into a plastic syringe, and then 5 mL of MilliQ water were added to remove unreacted molecules. Only the gravitational force acted on the system. Then 2 mL of solution containing MB at 12.5 μmol L^{-1} or Cu^{2+} ions at 0.15 mol L^{-1} were added. The solution took on average 3 min to flow through the hydrogels. After that, 6 mL of HCl 2.5 mol L^{-1} or HCl 1.0 mol L^{-1} were added in order to desorb MB or Cu^{2+} ions, respectively; the rinsing process took 3 min. Before adding 2 mL of MB or

Cu^{2+} solution for the next adsorption process, the hydrogels were re-conditioned with 6 mL of Tris–HCl buffer or MilliQ water, respectively, which took about 3 min. This step is important to re-activate the adsorption sites. Thus, one complete cycle took 9 min. The amount of MB or Cu^{2+} ions adsorbed and desorbed was evaluated by analyzing the filtrates by UV–Vis spectrophotometry. The adsorption/desorption cycles are schematically represented in the Supplementary Material SM5.

Results and discussion

Characterization of freeze-dried hydrogels

Table 1 shows the apparent density (ρ_{ap}), the compression modulus (ε), and swelling degree, SD, (g_{water}/$g_{adsorbent}$) values determined for the freeze-dried hydrogels or cryogels. The samples CMC:cPAA (0:100) were completely collapsed and sticky after freeze-drying, for this reason they were not characterized or used in the adsorption studies. Upon increasing the CMC content in the mixture, the resulting cryogels became denser, probably because bulk CMC is denser (1.6 g cm^{-3}) than bulk PAA (1.05 g cm^{-3}). The ε values determined for compression-strain curves showed a maximum of 141 ± 3 kPa for the composition CMC:cPAA 50:50 (Supplementary Material SM6), which is not the densest one. Generally, the compressive modulus (ε) depends on the ρ_{ap} values and on the cell morphology (open-cell, honeycomb, dendritic or cellular) (Gibson and Ashby 1997; Scotti and Dunand 2018). Figure 2 presents the SEM images obtained for the cryogels, they all present open cell morphology. However, the pores appeared on average larger as the content of CMC increased. Upon freezing, the ordered conformation and ice crystallization force the polymer chains to align and to associate, forming junction zones, which remain intact (Giannouli and Morris 2003). Thus, the SEM images indicate that ice expansion was more pronounced in CMC:cPAA mixtures with higher CMC contents.

The swelling degrees (SD) were determined from MilliQ water (pH 5.5) sorption curves during 4 h (Supplementary Material SM7). The SD values displayed in Table 1 varied from 65.9 ± 0.5 to 59 ± 2 g/g for the mixtures, but pure CMC hydrogels

Table 1 Apparent density (ρ_{ap}), compression modulus (ε) and swelling degree (SD) ($g_{water}/g_{adsorbent}$) values determined for the freeze-dried hydrogels at 22 ± 1 °C

CMC:cPAA	ρ_{ap} (kg.m^{-3})	ε (kPa)	SD ($g_{water}/g_{adsorbent}$) pH			SD ($g_{water}/g_{adsorbent}$) NaCl (mol L^{-1})	
			2.0	5.5	10.0	0.010	0.100
25:75	27 ± 1	69 ± 2	56 ± 3	55 ± 2	68 ± 3	65 ± 3	56 ± 2
50:50	27 ± 2	141 ± 3	67 ± 4	59 ± 2	71 ± 4	60 ± 3	64 ± 3
75:25	30 ± 1	108 ± 2	55 ± 3	57 ± 2	65 ± 3	56 ± 2	55 ± 3
100:0	34 ± 2	85 ± 3	56 ± 3	68 ± 2	80 ± 4	62 ± 3	67 ± 3

SD values were determined in MilliQ water (pH 5.5), 0.010 mol L^{-1} HCl (pH 2.0) and 0.0001 mol L^{-1} NaOH (pH 10.0). The effect of ionic strength was determined at pH 5.5 and 0.010 mol L^{-1} or 0.100 mol L^{-1} NaCl
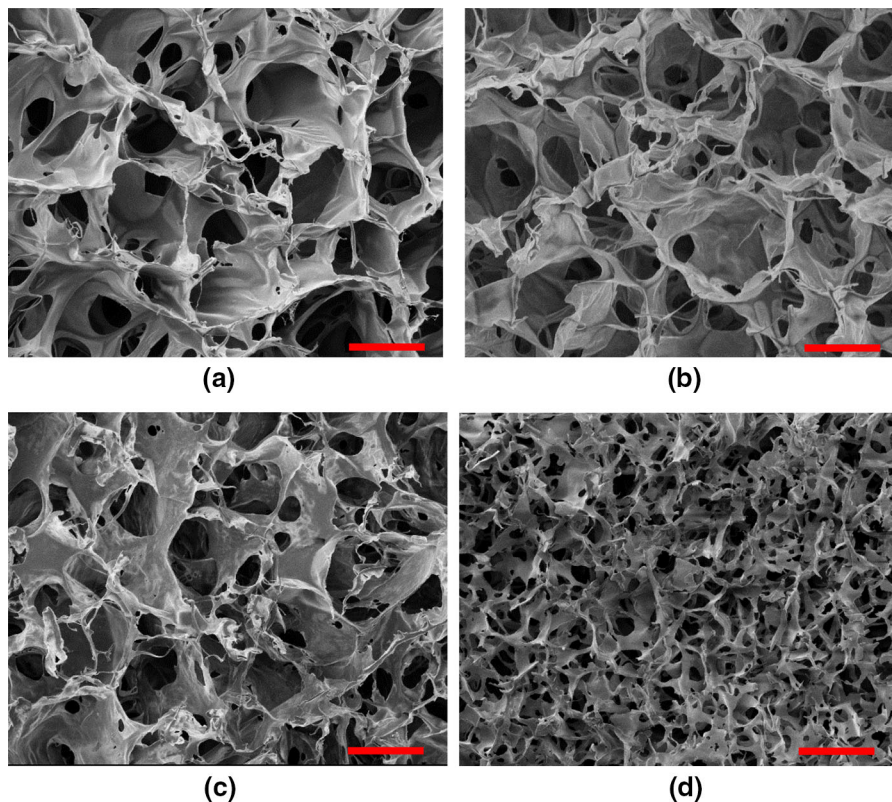
Fig. 2 SEM images obtained for CMC:cPAA cryogels: **a** 100:0, **b** 75:25, **c** 50:50, **d** 25:75. The red bar corresponds to 100 μm

behaved as superabsorbents with SD of 90 ± 2 g/g. CMC hydrogels prepared by ionizing radiation also behaved as superabsorbents, but in comparison to uncharged hydroxyethyl cellulose or hydroxypropyl cellulose hydrogels, the swelling behavior of CMC hydrogels was strongly dependent on the ionic strength of the medium (Fekete et al. 2014). The in situ radical polymerization of acrylic acid in the presence of CMC led to IPNs with maximum SD value of 18 g/g (Bajpai and Mishra 2004), showing that the use of cPAA as precursor to the development of CMC:cPAA hydrogels led to IPNs with higher swelling capacity. The SD values determined at pH 2.0 and pH 10.0 evidenced that the hydrogels under acidic conditions swollen at the same degree as in MilliQ water (Table 1). However, under alkaline

media the SD increased because ester bonds underwent hydrolysis. The SD values determined in 0.010 mol L^{-1} or 0.100 mol L^{-1} NaCl were similar to those determined in MilliQ water (Table 1), except for CMC:cPAA 100:0, which swelled less due to partial screening of carboxylate groups. Swelling tests with $CaCl_2$ and $FeCl_3$ were performed, but Ca^{2+} and Fe^{3+} adsorbed on CMC carboxylate groups, reducing the number of carboxylate groups available to interact with water molecules. Similar competitive process was observed for the swelling of hybrid hydrogel based on poly(N-isopropyl acrylamide-co-itaconic acid) containing octavinyl polyhedral oligomeric silsesquioxane as crosslinker (Eftekhari-Sis et al. 2018).

X-ray computed microtomography (CT) is a nondestructive reliable method for the simultaneous determination of porosity and the 3D reconstruction of porous networks (Vasić et al. 2007; Mariano et al. 2018). Figure 3 shows the computationally reconstructed 3D images from CT data using CTVox Bruker software for CMC:cPAA 100:0 and 50:50. The slices correspond to analyses of the total sample diameter (10 mm diameter), whereas the boxes of 2 mm × 2 mm (yellow squares) were colored according to the transformation function from attenuation to X-ray to color: 0–25% is void space; 25–37% in red; 38–50% in yellow; 50–100% in white, and linear increase of the color intensity. The red color stands for the highest amount of material and the white color for the lowest amount of material. The red color was more frequent in the composition 50:50 than in 100:0, corroborating with the mechanical behavior (Table 1), although the morphometric data (surface area, pore diameter, wall thickness and porosity) for CMC:cPAA at both compositions were similar.

The thermogravimetric (TG) curves are presented as Supplementary Material SM8 and the events with the corresponding mass losses and maximal temperatures (T_{max}) are compiled in Table 2. The mass loss in the first event (up to 100 °C) attributed to water release increased with the CMC content in the mixture, achieving 12% in the pure CMC cryogels. In comparison to pure CMC, the 2nd and 3rd events, which are probably related to side chain and backbone degradation, took place at higher T_{max} for the CMC:cPAA 75:25, whereas the 4th event (residual backbone degradation) occurred at higher T_{max} for the CMC:cPAA 75:25 and 50:50. The increase in the T_{max}

values indicate favorable interaction among polymer chains, probably ion–dipole interactions among cPAA carboxylate groups and CMC hydroxyl groups, increasing their chemical stability upon temperature increase.

Figure 4a, b show the FTIR-ATR spectra determined for CMC and cPAA powder, CMC:cPAA (100:0, 75:25, 50:50; 25:75) cryogels in the spectral range of 4000–600 cm^{-1} and of 2000–600 cm^{-1}, respectively. Figure 4b shows the general trend of typical bands of CMC decreased as the content of cPAA increased in the cryogels and vice versa. FTIR bands were attributed according to Silverstein et al. (Silverstein et al. 2014), the band at 1715 cm^{-1}, assigned to C=O stretching stemming from esters, was present in cPAA powder because the PAA chains are crosslinked through the esterification among the PAA carboxylic acid groups and erythritol hydroxyl groups. In comparison to the band at 1590 cm^{-1}, which was attributed to the asymmetric axial deformation of carboxylate groups stemming from CMC, the band at 1715 cm^{-1} became relatively weaker as the CMC content was increased. Noteworthy, in the CMC:cPAA (100:0) cryogels, the intensity of the band at 1715 cm^{-1} was the weakest. The bands at 1458 cm^{-1}, 1408 cm^{-1} and 1322 cm^{-1} were assigned to erythritol CH_2 scissor, symmetric axial deformation of C=O of esters and stretching of carboxylate C–O of CMC carboxylate groups. The signals in spectral region between 1200 and 870 cm^{-1} were attributed to C–O and C–C stretching vibrations of the CMC glucopyranose ring.

Regardless of the composition, the CMC:cPAA cryogels did not dissolve in water, they just became swollen. The CMC:cPAA (100:0) cryogels presented the highest SD (90 $\pm$ 2 $g_{water}/g_{cryogel}$) and the weakest band at 1715 cm^{-1}. The weak signals related to ester C=O stretching indicate that the esterification among CMC hydroxyl groups and citric acid was not pronounced. Probably, the electrostatic repulsion among the CMC chains pushed them apart, decreasing the esterification efficiency. However, even if the crosslinking took place at a low level, it was enough to keep all networks stable in water for 1 week. Thus, we can conclude that in the mixtures of cPAA and CMC, the CMC chains were able to permeate through the pre-existing crosslinked cPAA network, reducing the interchain electrostatic repulsion and then undergoing esterification with citric acid in the entangled state,
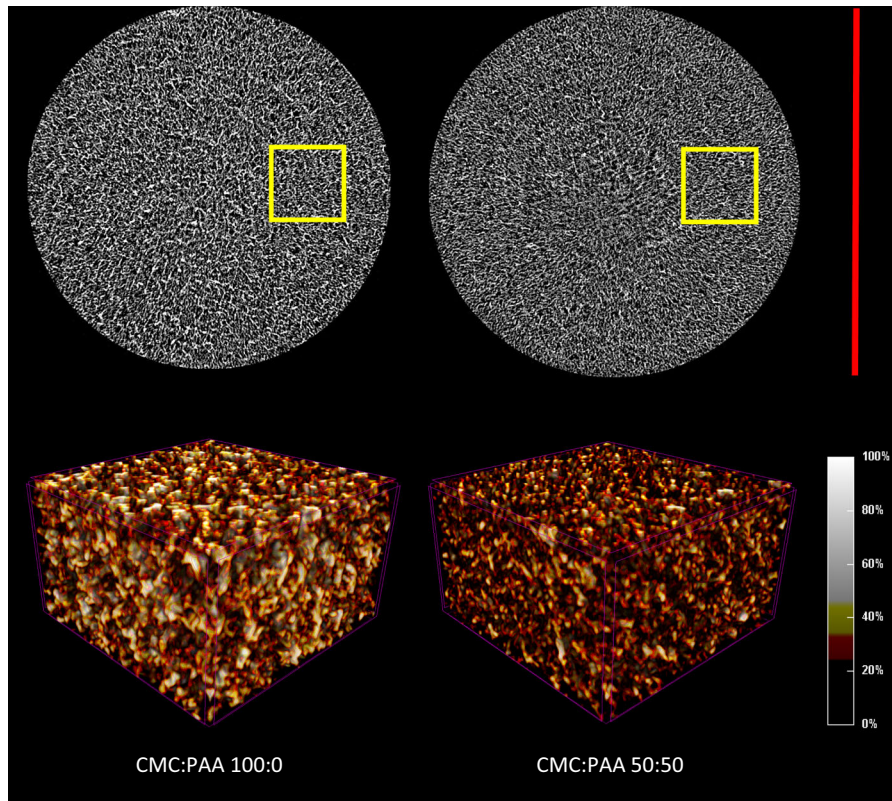
CMC:cPAA	Surface Area (m². g⁻¹)	Diameter (µm)	Thickness (µm)	Porosity (%)
50:50	1.19 ± 0.05	34.4 ± 0.1	55.0 ± 0.1	96.8
100:0	0.91 ± 0.03	36.2 ± 1.7	58.3 ± 3.3	94.9

Fig. 3 Computer reconstructed 3D models from CT data of cylindrical CMC:cPAA 100:0 and 50:50 cryogels. For the longitudinal slices the red bar corresponds to 10 mm, whereas the boxes dimensions are 2.0 mm × 2.0 mm (in yellow) and 1.2 mm high, colored according to the same transformation function from attenuation to X-ray to color: 0–25% is void space; 25–37% in red; 38–50% in yellow; 50–100% in white, and linear increase of the color intensity

**Table 2** TGA data for CMC:cPAA cryogels

For each event, the mass loss in wt% was indicated with maximal temperature in parentheses. The first event was attributed to water release and took place up to 100 °C

CMC:cPAA	1st Event (%)	2nd Event	3rd Event	4th Event	5th Event	Ashes (%)
100:0	12	17% (229 °C)	24% (299 °C)	11% (440 °C)	18% (803 °C)	18
75:25	10	12% (238 °C)	31% (307 °C)	9% (449 °C)	22% (789 °C)	16
50:50	8	12% (225 °C)	23% (315 °C)	22% (493 °C)	17% (758 °C)	18
25:75	5	15% (214 °C)	17% (316 °C)	27% (374 °C)	26% (754 °C)	10
0:100	5	23% (238 °C)	53% (394 °C)	– –	– –	19
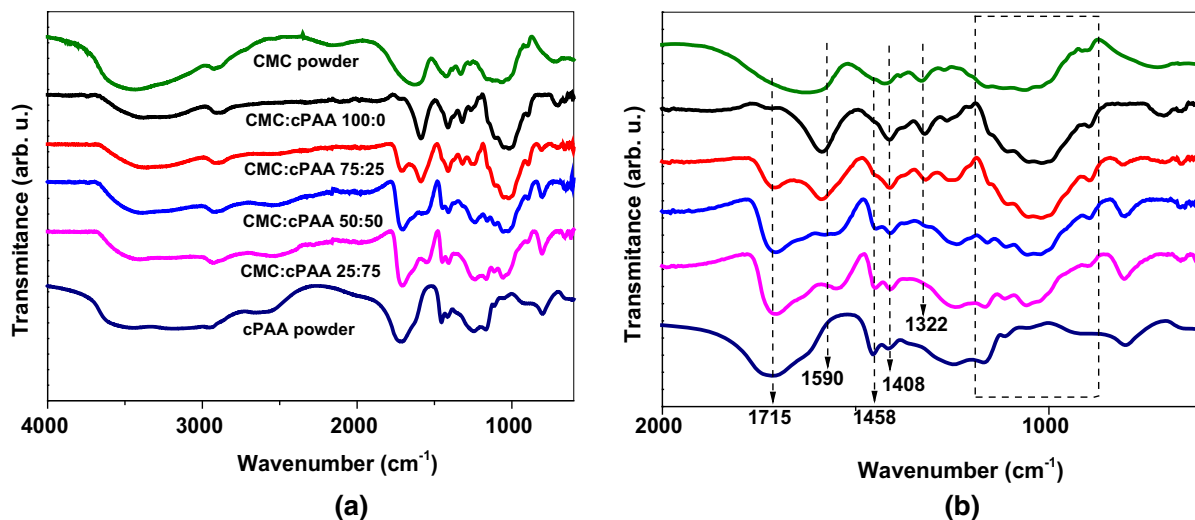
Fig. 4 FTIR-ATR spectra determined for CMC and cPAA powder, CMC:cPAA (100:0, 75:25, 50:50; 25:75) cryogels in the spectral range of **a** 4000–600 cm^{-1} and **b** 2000–600 cm^{-1}

Fig. 5 Schematic representation of isolated and crosslinked CMC chains (red lines) with citric acid (black lines) and crosslinked CMC chains in the presence of cPAA (blue lines), forming full IPNs. The photos show cylindrical CMC:cPAA 100:0 and 50:50 cryogels immersed in water (30 min contact)
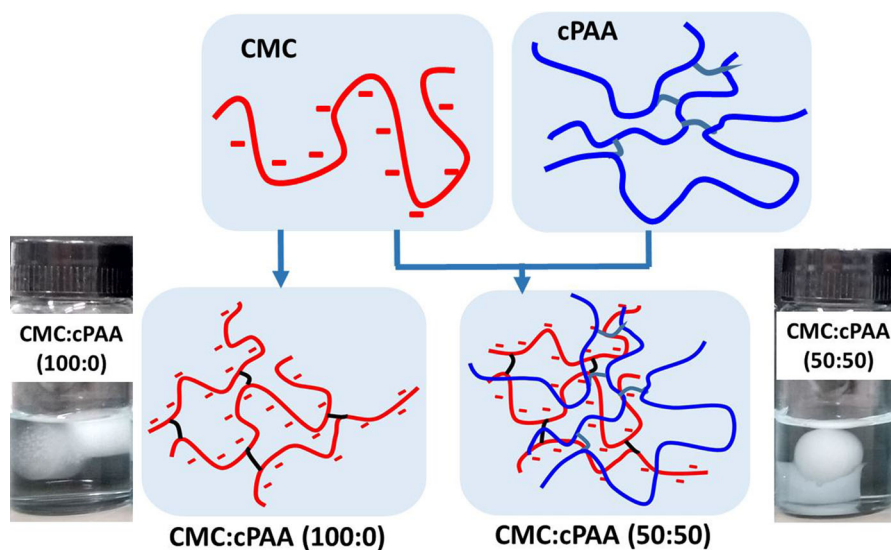
forming full IPN (Fig. 5). This process explains the increase of the compression modulus (Table 1) and the T_{max} values (Table 2) for the compositions CMC:cPAA 50:50 and 75:25.

The gel contents determined for CMC:cPAA hydrogels amounted to $86 \pm 3\%$, regardless of the composition, indicating a high degree of crosslinking in the full IPNs. As a control experiment, CMC:cPAA 50:50 hydrogels were prepared in the absence of citric acid and HPS. During dry heat treatment ester bonds might be formed between carboxyl groups and hydroxyl groups of CMC without citric acid.

However, the gel content of $73 \pm 3\%$, indicated that it happened to a lower extent. Similar behavior was observed for xanthan hydrogels prepared in the absence of citric acid (Bueno et al. 2013).

Adsorption of methylene blue on hydrogels

Figure 6a shows the removal capacity of CMC:cPAA hydrogels for the MB initial concentration (C_i) range from 0.5 to 4 mg L^{-1}, after 24 h contact under shaking. On average, CMC:cPAA 25:75, 50:50, 75:25 and 100:0 hydrogels presented removal capacities of
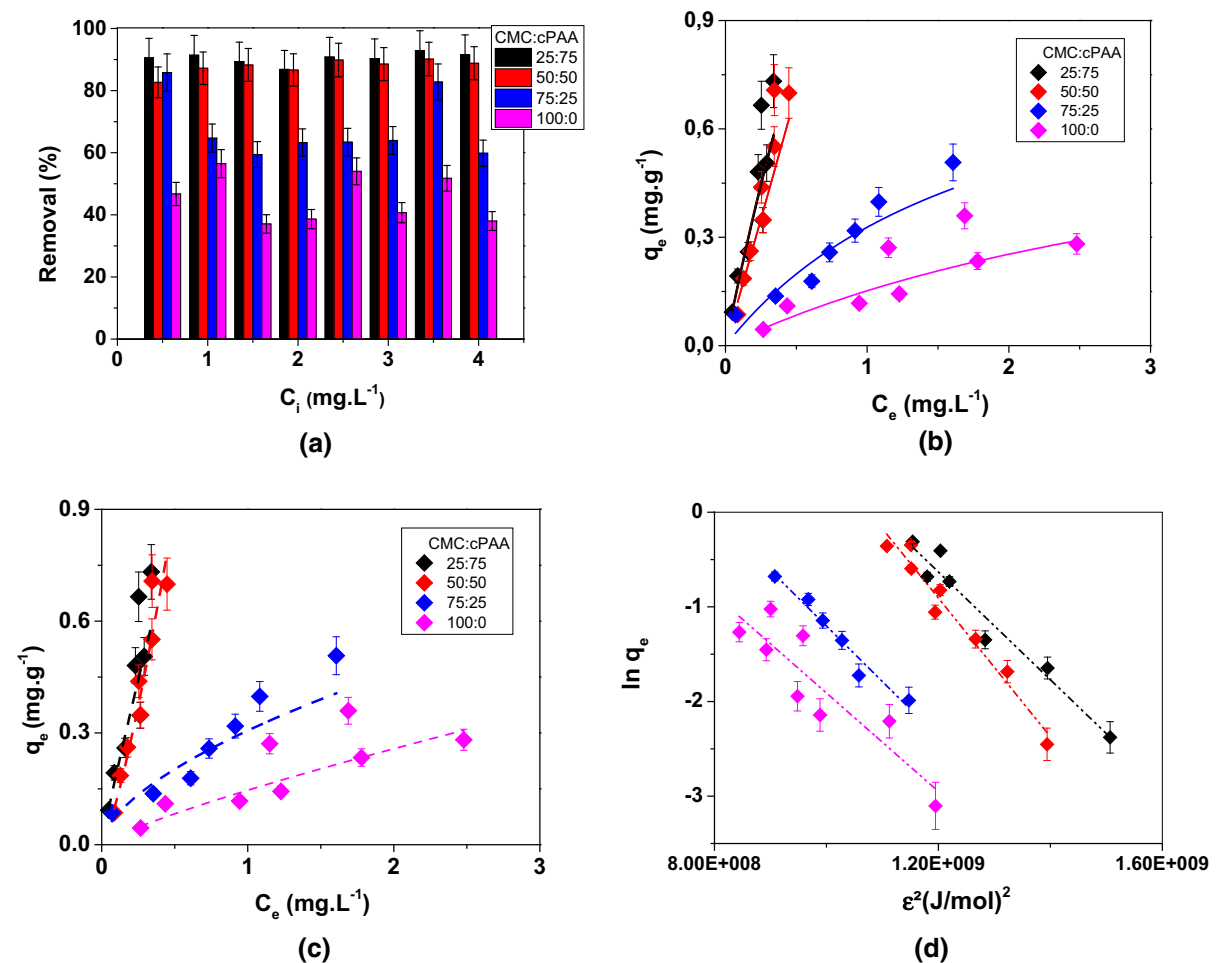
Fig. 6 Adsorption of MB on CMC:cPAA hydrogels 25:75 (black), 50:50 (red), 75:25 (blue) and 100:0 (magenta) as a function of C_i, mean mass of aerogel (0.020 ± 0.002) g, pH 7 (Tris–HCl buffer), volume of MB solution was 5 mL, 24 h contact under shaking, at 24 ± 1 °C. **a** Removal capacity,

b adsorption isotherm along with nonlinear fitting with Langmuir model, **c** adsorption isotherm along with nonlinear fitting with Freundlich model, **d** linear fitting of experimental data shown in (**b**) and (**c**) with D–R model

$90 \pm 6\%$, $88 \pm 5\%$, $68 \pm 5\%$ and $45 \pm 4\%$, respectively. Figure 6b, c present the adsorption isotherms of MB on hydrogels (20 ± 2 mg dried basis and 5 mL solution), along with the nonlinear fittings for Langmuir and Freundlich models. In order to estimate the adsorption energy (E_{ads}), the experimental data were also fitted with the Dubinin–Radushkevitch (D–R) linear model. The equations and the corresponding linearized forms of Langmuir, Freundlich and D–R adsorption models are provided in the Supplementary Material SM9. C_e, q_e and q_{max} stand for equilibrium concentration (mg L^{-1}), adsorption at equilibrium (mg g^{-1}) and maximum adsorption capacity, respectively (Foo and Hameed 2010; Tran et al. 2017).

Table 3 shows the parameters determined from nonlinear fittings corresponding to Langmuir and Freundlich models, along with the χ^2 values, and from linear fitting with D–R model along with the R^2 values. The criteria for the best fitting are the smallest χ^2 value and the R^2 value closest to 1. The linear fits for Langmuir and Freundlich are available as Supplementary Material SM10; the linear fitting with Langmuir model yielded poor quality, whereas the linear fitting with Freundlich model showed better correlation coefficients (R^2) and the fitting parameters n and K_F were similar to those determined from nonlinear fittings. The q_{max} and affinity constant (K_L) values determined from Langmuir and D–R models (Table 3)

Table 3 Adsorption of MB onto CMC:cPAA hydrogels

CMC:cPAA	Nonlinear fitting		Linear
	Langmuir	Freundlich	D–R
25:75	q_{max}= 390 mg g^{-1}	n = 0.9252	q_{max}= 493 mg g^{-1}
	K_L = 2.76 L g^{-1}	K_F = 1.595 $\left(\frac{mg}{L \times g}\right)\Big/\left(\frac{mg}{L \times g}\right)^{\frac{1}{n}}$	E = 9.4 kJ mol^{-1}
	χ^2 = 0.012	χ^2 = 5.3122	R^2 = 0.944
50:50	q_{max} = 613 mg g^{-1}	n = 1.2718	q_{max} = 2643 mg g^{-1}
	K_L = 5.04 L mg^{-1}	K_F = 2.173 $\left(\frac{mg}{L \times g}\right)\Big/\left(\frac{mg}{L \times g}\right)^{\frac{1}{n}}$	E = 9.3 kJ mol^{-1}
	χ^2 = 0.006	χ^2 = 2.4323	R^2 = 0.956
75:25	q_{max}= 2.99 mg g^{-1}	n = 0.5961	q_{max}= 107 mg g^{-1}
	K_L = 0.13 L mg^{-1}	K_F = 0.306 $\left(\frac{mg}{L \times g}\right)\Big/\left(\frac{mg}{L \times g}\right)^{\frac{1}{n}}$	E = 9.2 kJ mol^{-1}
	χ^2 = 0.0012	χ^2 = 5.4044	R^2 = 0.950
100:0	q_{max} = 0.61 mg g^{-1}	n = 0.8165	q_{max} = 26.83 mg g^{-1}
	K_L = 0.042 L mg^{-1}	K_F= 0.146 $\left(\frac{mg}{L \times g}\right)\Big/\left(\frac{mg}{L \times g}\right)^{\frac{1}{n}}$	E = 9.0 kJ mol^{-1}
	χ^2 = 0.043	χ^2 = 8.3588	R^2 = 0.7794

Parameters determined from nonlinear and linear fittings corresponding to Langmuir, Freundlich and D–R models, along with the χ^2 and R^2 values

clearly indicated that the CMC:cPAA 25:75 and 50:50 hydrogels as the best adsorbents for MB, although the E_{ads} values determined for all hydrogels were high, on the order of 9 kJ mol^{-1}, which might be typical for electrostatic interaction or ion–dipole interaction. CMC:cPAA 25:75 and 50:50 hydrogels also presented the highest adsorption capacity (K_F) values and the largest n values, indicating low heterogeneity. In this work, the highest q_{max} values amounted to 613 mg g^{-1} for MB on CMC:cPAA 50:50 hydrogels. This value is one order of magnitude higher than that determined for CMC coated magnetic nanoparticles (q_{max} value of 22.7 mg g^{-1}) (Zirak et al. 2017), and similar to that observed for grafted dimethyldiallylammonium on crosslinked CMC particles (q_{max} value of 710.50 mg g^{-1}) (Lin et al. 2016).

The results in Table 3 show that the q_{max} values decreased as the CMC content in the mixture increased. This effect might be correlated to the increase of charge density in the hydrogels, as evidenced by the vibrational band at 1519 cm^{-1} assigned to the asymmetric axial deformation of carboxylate groups in the FTIR spectra (Fig. 4b). MB molecules have three pK$_a$ values, namely, 1.7, 4.5 and 5.9; the ionization equilibria corresponding to each pK$_a$ are presented as Supplementary Material S11 (Impert et al. 2003). The adsorption experiments took place at pH 7 (buffer Tris–HCl), at this pH the MB molecules are negatively charged and the CMC carboxylic acid is also deprotonated, making the adsorption unfavorable due to electrostatic repulsion. Thus, one can conclude that the adsorption of MB molecules on CMC:cPAA 25:75 and 50:50 are driven by interactions among dipoles stemming from cPAA ester groups and anions from MB molecules. When CMC:cPAA 0:100 hydrogels were inserted into MB solution, there was practically no adsorption even after 24 h contact because it collapsed completely, reducing the surface area dramatically. Therefore, in comparison to pure cPAA hydrogels or pure CMC hydrogels, the combination of cPAA with CMC chains at 50:50 ratio led to IPN hydrogels with superior mechanical properties, large surface area and high adsorption capacity.

The adsorption kinetics of MB onto CMC:cPAA hydrogels was systematically investigated for MB at 0.5 mg L^{-1} and 4.0 mg L^{-1}. The amounts of adsorbate uptake per mass of adsorbent at equilibrium and at any time t (min) are denoted as q_e and q_t, respectively. The adsorption kinetics behavior can be quantitatively evaluated using the pseudo-first order and pseudo-second order equations, Eqs. 4 and 5, respectively:

$$\ln(q_e - q_t) = -k_1 t + \ln q_e \tag{4}$$

$$\frac{t}{q_t} = \left(\frac{1}{q_e}\right)t + \frac{1}{k_2 q_e^2} \tag{5}$$

where k_1 and k_2 are adsorption rate constants.

Figure 7a–c show the q_t values as function of time for MB at 0.5 mg L^{-1} and the corresponding fittings with pseudo-1st order and pseudo-2nd order equations, respectively. Figure 7d–f show the q_t values as function of time for MB at 4.0 mg L^{-1} and the corresponding fittings with pseudo-1st order and pseudo-2nd order equations, respectively. The fitting parameters in Table 4 indicated that for both MB concentrations the pseudo-2nd order model was the best one because the calculated and experimental q_e values were similar and R^2 values were closer to 1. Similar behavior was reported for MB onto grafted dimethyldiallylammonium on crosslinked CMC particles (Lin et al. 2016). It means that the adsorption process depends on both MB concentration and amount of adsorbent.

The adsorption rate constant k_2 values for equilibrium condition was larger for the more dilute MB solution (0.5 mg L^{-1}), indicating that mass transport plays an important role. The intraparticle diffusion model (IPD) proposed by Weber and Morris (Weber and Morris 1963) has been widely applied for the analysis of mass transfer from solution to the solid–liquid interface and the diffusion of the adsorbate into the porous media:

$$q = k_{intra}t^{0.5} \qquad (6)$$

where k_{intra} is the diffusion rate, which is proportional to the diffusion coefficient of the adsorbate.

Figure 8a, b show the dependence of q_t on t$^{0.5}$ for MB at 0.5 mg L^{-1} and 4.0 mg L^{-1}, respectively. In general, two different slopes were obtained by piecewise linear regression (dot lines), which correspond to different consecutive stages of mass transport with decreasing rate. The first sharper linear region is a fast stage that can be related to the free diffusion of MB molecules from the solution towards to the external surface of CMC:cPAA hydrogels. The second region, a slower one, may be assigned to the gradual diffusion of MB molecules to the hydrogel interior, where there are physical constraints. The change from transport rate regime took place after approximately 4 h. Table 5 shows that the k_{intra} values decreased one order of magnitude from the 1st to the 2nd adsorption stage and increased one order of magnitude from the MB concentration 0.5–4.0 mg L^{-1}. The smallest k_{intra} values were observed for CMC:cPAA (100:0)

hydrogels due to electrostatic repulsion. Figure 8c shows the pristine CMC:cPAA 50:50 freeze-dried hydrogel (9 mm diameter) before and after 10 min contact with MB solution (4.0 mg L^{-1}); the diameter increased to 12 mm, evidencing the high swelling capacity. It is also clear that the MB molecules are predominantly on the surface, whereas the interior is still white.

Adsorption of Cu^{2+} ions on hydrogels

Among all hydrogels the CMC:cPAA 50:50 hydrogels presented the highest ε value (141 ± 3) kPa (Table 1) and was the best adsorbent for MB (q_{max} = 613 mg g^{-1}). Based on these results, the CMC:cPAA 50:50 hydrogels were chosen as adsorbents for the adsorption of Cu^{2+} ions. Figure 9a shows the adsorption isotherm determined at 24 ± 1 °C, pH 4.5, 2 h contact under shaking, along with nonlinear fitting with Freundlich model, the corresponding liner fitting is provided in the Supplementary Material SM12. Figure 9b, c present the linear fittings with Langmuir and D–R models; the corresponding nonlinear fittings did not converge. Table 6 shows the fitting parameters. The q_{max} values determined from Langmuir and D–R models amounted to 250 mg g^{-1} and 267.8 mg g^{-1}, respectively. For comparison, beads of CMC crosslinked with epichlorohydrin presented q_{max} of 6.5 × 10^{-3} mol g^{-1} at pH 7 (Yang et al. 2010). The q_{max} of Cu^{2+} ions on chitosan–alginate beads at pH ∼ 4 was 67.66 mg g^{-1} (Ngah and Fatinathan 2008). The maximum Cu^{2+} ions uptake by dried sunflower leaves was 89.37 mg g^{-1} (Benaïssa and Elouchdi 2007). Therefore, the CMC:cPAA hydrogels presented high adsorption capacity towards Cu^{2+} ions. At pH 4.5 the CMC carboxylate groups are partially deprotonated because its pKa ∼ 4.0. Therefore, the adsorption might be driven by interactions among Cu^{2+} ions and CMC carboxylate or hydroxyl groups, corroborating with the E$_{ads}$ value of 4.83 kJ mol^{-1}. The linear fitting with Freundlich model presented poorer quality than those determined with Langmuir or D–R models (Table 6).

In order to evaluate the effect of the presence of other cations on the adsorption of Cu^{2+} ions on CMC:cPAA 50:50 hydrogels, the q$_e$ values were determined for Cu^{2+} (C$_i$ = 0.15 mol L^{-1} or 37.5 g L^{-1}) in the presence of 0.100 mol L^{-1} NaCl or 0.100 mol L^{-1} ZnSO$_4$. ZnSO$_4$ was chosen because it
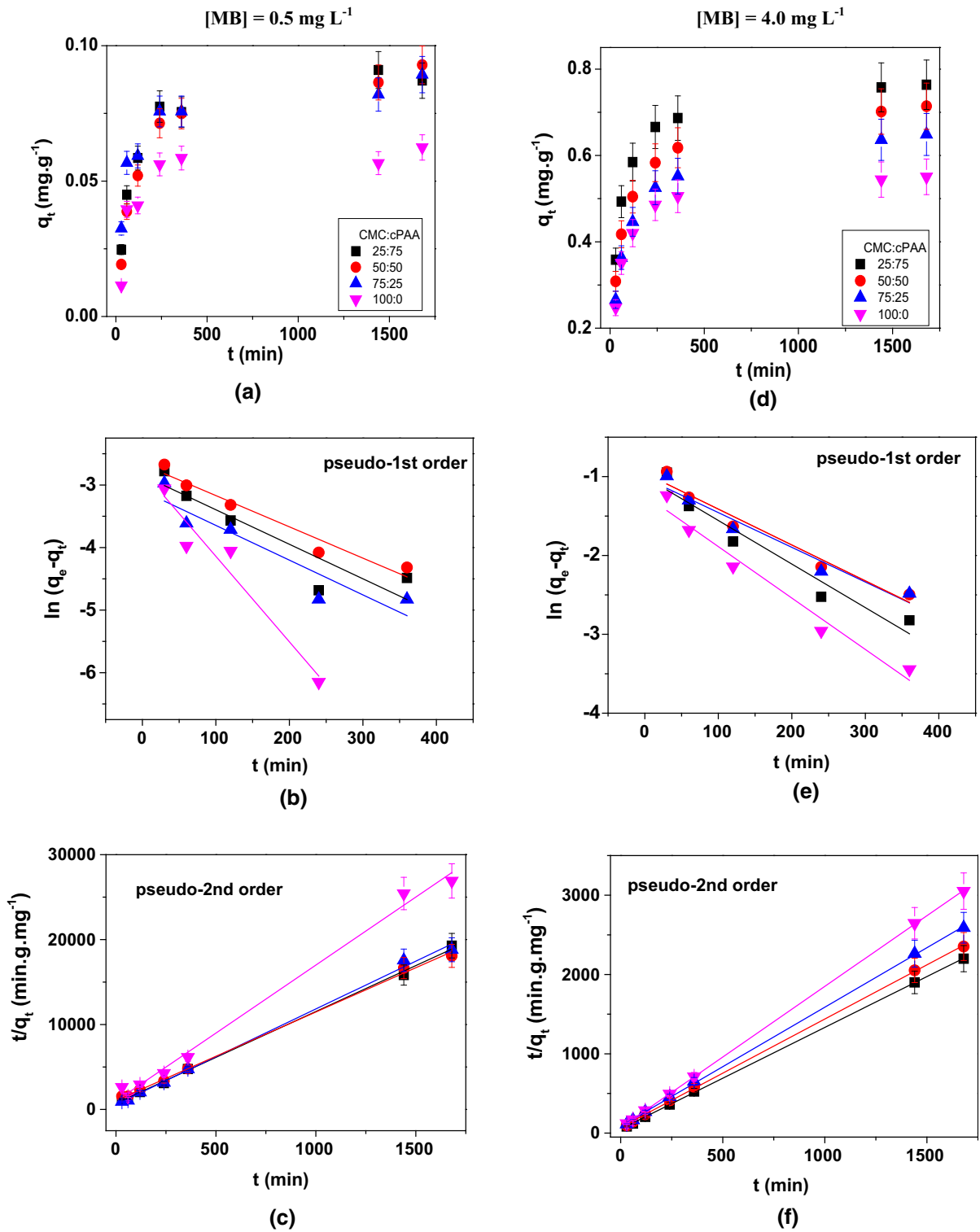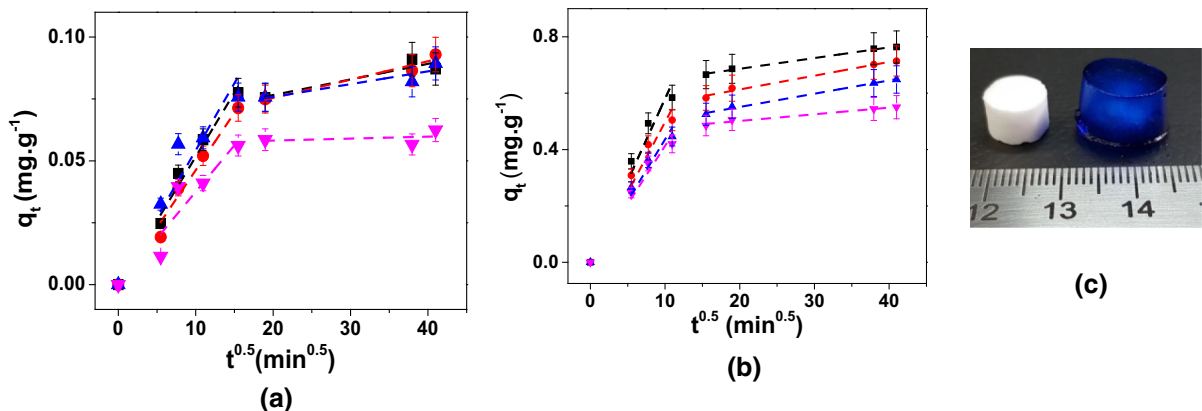
Fig. 7 **a** Dependence of q_t values on time for MB at **a** 0.5 mg L^{-1} and **d** 4.0 mg L^{-1} and the corresponding fittings with **b**, **e** pseudo-1st order and **c**, **f** pseudo-2nd order equations

Table 4 Fittings parameters determined for the adsorption kinetics of MB at (a) 0.5 mg L^{-1} and (d) 4.0 mg L^{-1} on CMC:cPAA hydrogels with pseudo-1st order and pseudo-2nd order equations

CMC:PAA	Pseudo-1st order				Pseudo-2nd order			
	k_1 (10^{-3} min^{-1})	q_e calc (10^{-3} mg g^{-1})	q_e exp (10^{-3} mg g^{-1})	R^2	k_2 (g mg^{-1} min^{-1})	q_e calc (10^{-3} mg g^{-1})	q_e exp (10^{-3} mg g^{-1})	R^2
0.5 mg L^{-1} μM								
25:75	5.5	0.059	0.091	0.7843	0.160	0.093	0.091	0.9983
50:50	5.0	0.069	0.086	0.9370	0.104	0.096	0.086	0.9974
75:25	5.5	0.045	0.082	0.8239	0.217	0.089	0.082	0.9962
100:0	13.7	0.062	0.057	0.9127	0.261	0.062	0.057	0.9918
4.0 mg L^{-1} μM								
25:75	5.53	0.366	0.758	0.9217	0.032	0.780	0.758	0.9999
50:50	4.55	0.384	0.702	0.9573	0.026	0.732	0.702	0.9997
75:25	4.4	0.346	0.636	0.9387	0.026	0.666	0.636	0.9997
100:0	6.52	0.291	0.544	0.9596	0.046	0.561	0.544	0.9999

Fig. 8 Dependence of q_t on t$^{0.5}$ for the adsorption of MB at **a** 0.5 mg L^{-1} and **b** 4.0 mg L^{-1}, on CMC:cPAA hydrogels 25:75 (black), 50:50 (red), 75:25 (blue) and 100:0 (magenta). The lines are the linear regressions. **c** Photograph of pristine CMC:cPAA 50:50 freeze-dried hydrogel before and after 10 min contact with MB solution (4.0 mg L^{-1})

is soluble and colorless. NaCl increased the q_e value by 3%; such change is not significant. Nevertheless, in the presence of 0.100 mol L^{-1} ZnSO$_4$, the q_e values decreased on average 20%, indicating that Cu^{2+} and Zn^{2+} ions compete for the CMC carboxylate groups.
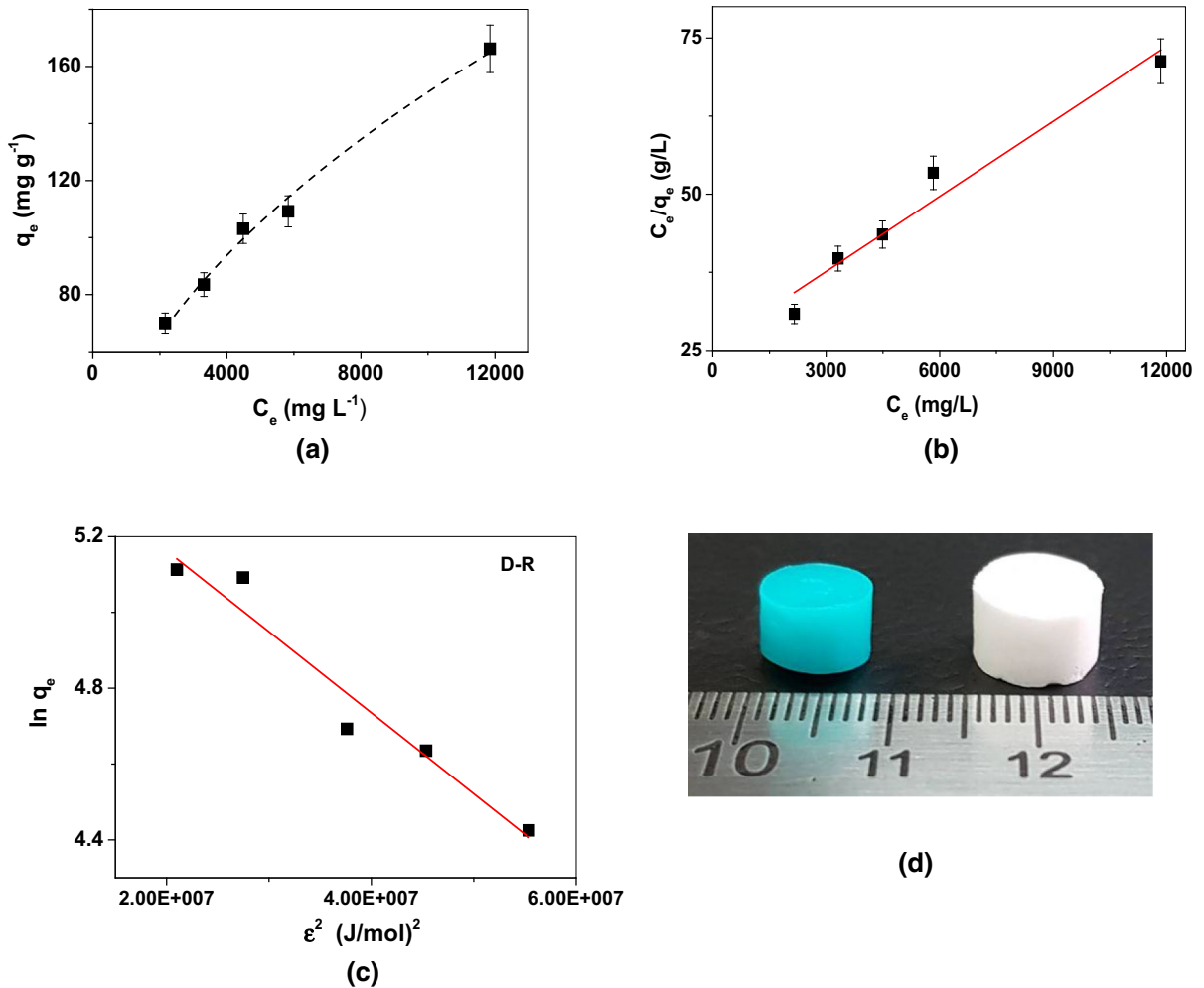
Figure 9d shows the pristine CMC:cPAA 50:50 freeze-dried hydrogel before and after 10 min contact with Cu^{2+} solution (37.5 g L^{-1}). In contrast to the swelling behavior observed after contact with MB solution, in this case, the hydrogels contracted from 9 mm diameter (pristine) to 7 mm. The high ionic strength and adsorption of Cu^{2+} ions screened the CMC carboxylate groups, causing contraction. Similar

effects were reported for CMC hydrogels, where the SD values in deionized water and in CaCl$_2$ at 0.1 mol dm^3 amounted to 200 g g^{-1} and ~ 30 g g^{-1}, respectively (Fekete et al. 2014).

Figure 10a–c show the q_t values as function of time for Cu^{2+} ions at 12.5 g L^{-1} (black symbols) and 37.5 g L^{-1} (red symbols), the pseudo-1st order and pseudo-2nd order fittings, respectively. The fitting parameters in Table 7 indicated that for both Cu^{2+} concentrations the pseudo-2nd order model was the best one because the calculated and experimental q_e values were closer and R^2 values were nearer to 1. Similar behavior was also observed for the adsorption

**Table 5** k_{intra} values determined from the linear regressions in Fig. 8a, b

CMC:PAA	1st slope		2nd slope	
	k_{intra} (10^{-3} mg g^{-1} min$^{-0.5}$)	R^2	k_{intra} (10^{-3} mg g^{-1} min$^{-0.5}$)	R^2
0.5 mg L^{-1}				
25:75	0.0052 ± 0.0002	0.9948	0.00063 ± 0.00002	0.7354
50:50	0.0046 ± 0.0002	0.9934	0.00074 ± 0.00002	0.8908
75:25	0.0054 ± 0.0005	0.9710	0.00052 ± 0.00002	0.6323
100:0	0.0037 ± 0.0004	0.9697	0.00080 ± 0.00002	0.7960
4.0 mg L^{-1}				
25:75	0.058 ± 0.004	0.9870	0.0038 ± 0.0002	0.9916
50:50	0.050 ± 0.003	0.9887	0.0049 ± 0.0004	0.9801
75:25	0.044 ± 0.002	0.9912	0.0047 ± 0.0002	0.9636
100:0	0.041 ± 0.002	0.9898	0.0024 ± 0.0003	0.9924

(a)

(b)

(c)

(d)

Fig. 9 **a** Adsorption isotherm determined at 24 ± 1 °C, pH 4.5, 2 h contact under shaking, along with nonlinear fitting with Freundlich model, and linear fittings with **b** Langmuir and **c** D–R models. **d** Photograph of pristine CMC:cPAA 50:50 freeze-dried hydrogel before and after 10 min contact with Cu^{2+} solution (37.5 g L^{-1})

Table 6 Adsorption of Cu^{2+} ions onto CMC:cPAA hydrogels

Linear fitting			Non-linear
Langmuir	D–R	Freundlich	Freundlich
q_{max}= 250 mg g^{-1}	q_{max}= 267.8 mg g^{-1}	$n = 2.27$	$n = 1.92$
K_L= 1.56 × 10^{-4} L/g	E_{ads} = 4.84 kJ mol^{-1}	K_F= 2.59 $\left(\frac{mg}{L \times g}\right) \Big/ \left(\frac{mg}{L \times g}\right)^{\frac{1}{n}}$	K_F= 1.26 $\left(\frac{mg}{L \times g}\right) \Big/ \left(\frac{mg}{L \times g}\right)^{\frac{1}{n}}$
$R^2 = 0.9506$	$R^2 = 0.9340$	$R^2 = 0.9216$	$\chi^2 = 14.7382$

Parameters determined from nonlinear fitting with Freundlich model and linear fittings corresponding to Langmuir, Freundlich and D–R models, along with the χ^2 and R^2 values
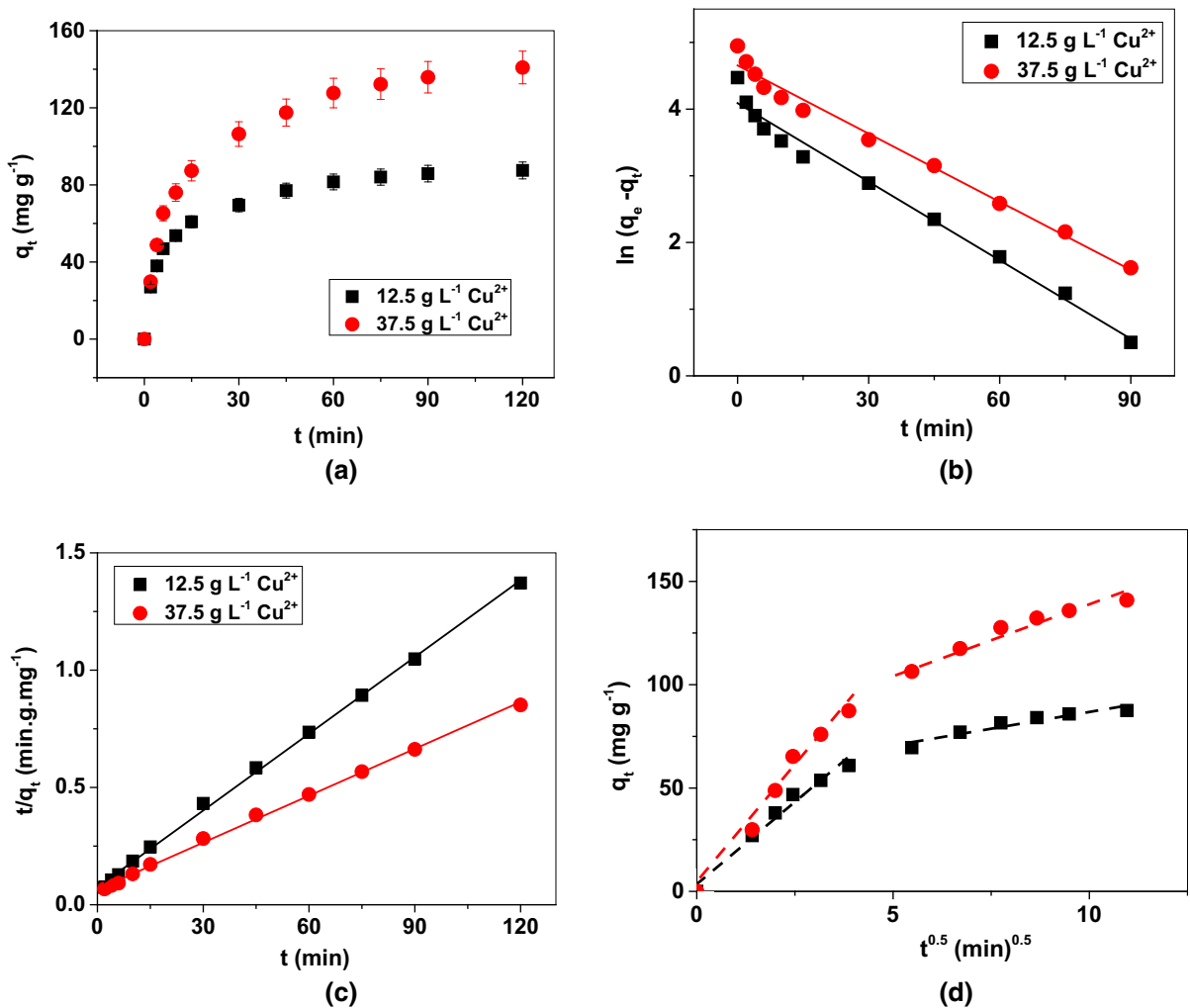
Fig. 10 **a** Dependence of q_t values on time for Cu^{2+} ions at 12.5 g L^{-1} (black) and 37.5 g L^{-1} (red) on CMC:cPAA 50:50 and the corresponding fittings with **b** pseudo-1st order, **c** pseudo-2nd order and **d** IPD equations

Table 7 Fittings parameters determined for the adsorption kinetics of Cu^{2+} ions at 12.5 g L^{-1} and 37.5 g L^{-1} on CMC:cPAA 50:50 with pseudo-1st order, pseudo-2nd order and IPD equations

	$[Cu^{2+}]$ 12.5 (g L^{-1})	$[Cu^{2+}]$ 37.5 (g L^{-1})
Pseudo-1st order		
k_1 (min^{-1})	0.0393	0.034
q_e calc (mg g^{-1})	59.7	105
q_e exp (mg g^{-1})	90	140
R^2	0.9814	0.9837
Pseudo-2nd order		
k_2 (g mg^{-1} min^{-1})	0.0016	6.8×10^{-4}
q_e calc (mg g^{-1})	91.7	150
q_e exp (mg g^{-1})	90	140
R^2	0.9986	0.9974
IPD		
k_{intra} fast (mg g^{-1}.min$^{-0.5}$)	15.93	23.74
R^2	0.9703	0.9949
k_{intra} slow (mg g^{-1}.min$^{-0.5}$)	3.239	6.324
R^2	0.8835	0.9352

of Cu^{2+} ions onto chitosan–alginate beads (Ngah and Fatinathan 2008) or dried sunflower leaves (Benaïssa and Elouchdi 2007).

The adsorption rate constant k_2 value was larger for the lowest Cu^{2+} ions concentration (12.5 g L^{-1}), indicating that the mass transport relevance for the adsorption process. Figure 10d shows the experimental data fittings with the IPD model. The k_{intra} values determined for the fast and slow stages are presented in Table 7. At the beginning the Cu^{2+} ions diffuse from the bulk solution to the hydrogel surface, interact with CMC carboxylate or hydroxyl groups on the surface. After approximately 30 min, the external surface has many adsorbing sites occupied by already adsorbed Cu^{2+} ions, thus the arriving Cu^{2+} ions have to diffuse into the hydrogel macropores, where the physical hindrance make the adsorption process slower. In contrast, the transition from fast to slow regime took 4 h in the adsorption process of MB molecules on CMC:cPAA 50:50 hydrogels, due to less favored interactions among adsorbate and substrate.

Desorption and recycling

The desorption of MB or Cu^{2+} ions from the hydrogels was achieved by rinsing with 6 mL of HCl 2.5 mol L^{-1} or HCl 1.0 mol L^{-1}, respectively; the rinsing process took 3 min. In both cases, the acid medium increased the adsorbate solubility and protonated all carboxylate groups, favoring desorption and CMC:cPAA hydrogels recycling (Supplementary Material Figure SM13). After five adsorption/desorption cycles of MB and Cu^{2+}, the CMC:cPAA 50:50 hydrogels kept 90% of the original removal capacity, indicating the potential of these hydrogels. For practical purposes, the cost-effectiveness relationship was estimated. On average, for lab consumables the local costs of CMC and cPAA are US$ 10.00 per kg and US$ 17.00 per kg, respectively. Therefore, one kg of dried CMC:cPAA hydrogel would cost US$ 13.50. However, due to the possibility of recycling five times, the cost would be reduced to US$ 2.70.

Conclusions

Full IPN hydrogels of CMC:cPAA were prepared using commercial PAA single IPN hydrogels as precursor and citric acid as crosslinker for CMC chains. This simple strategy avoided the use of toxic crosslinkers and led to full IPNs with improved mechanical (141 ± 3 kPa) and swelling properties (58 ± 2 g$_{water}$ g^{-1}) in comparison to each single component IPN. The CMC:cPAA 50:50 hydrogels were particularly efficient for the adsorption of MB dye (613 mg g^{-1}) and Cu^{2+} ions (250 mg g^{-1}), pointing at the potentiality of these hydrogels as adsorbents for preconcentration and removal of pollutants. Moreover, the excellent recyclability makes them attractive because it allows reducing the costs significantly. The porous structure and biocompatibility of both components open the possibility to apply CMC:cPAA hydrogels in the biomedical field as drug carriers and scaffolds for tissue engineering.

References

Bajpai AK, Mishra A (2004) Ionizable interpenetrating polymer networks of carboxymethyl cellulose and poly(acrylic acid): evaluation of water uptake. J Appl Polym Sci 93:2054–2065. https://doi.org/10.1002/app.20674

Bajpai AK, Mishra A (2005) Preparation and characterization of tetracyclin-loaded interpenetrating polymer networks of carboxymethyl cellulose and poly(acrylic acid): water sorption and drug release study. Polym Int 54:1347–1356. https://doi.org/10.1002/pi.1839

Benaïssa H, Elouchdi MA (2007) Removal of copper ions from aqueous solutions by dried sunflower leaves. Chem Eng Process Process Intensif 46:614–622. https://doi.org/10.1016/j.cep.2006.08.006

Bueno VB, Petri DFS (2014) Xanthan hydrogel films: molecular conformation, charge density and protein carriers. Carbohydr Polym 101:897–904. https://doi.org/10.1016/j.carbpol.2013.10.039

Bueno VB, Bentini R, Catalani LH, Petri DFS (2013) Synthesis and swelling behavior of xanthan-based hydrogels. Carbohydr Polym 92:1091–1099. https://doi.org/10.1016/j.carbpol.2012.10.062

Cai Y, Yuan F, Wang X et al (2017) Synthesis of core–shell structured Fe_3O_4@carboxymethyl cellulose magnetic composite for highly efficient removal of Eu(III. Cellulose 24:175. https://doi.org/10.1007/s10570-016-1094-8

Crini G (2005) Recent developments in polysaccharide-based materials used as adsorbents in wastewater treatment. Prog Polym Sci 30:38–70. https://doi.org/10.1016/j.progpolymsci.2004.11.002

Dai H, Ou S, Huang Y, Liu Z, Huang H (2017) Enhanced swelling and multiple-responsive properties of gelatin/sodium alginate hydrogels by the addition of carboxymethyl cellulose isolated from pineapple peel. Cellulose 25:593–606. https://doi.org/10.1007/s10570-017-1557-6

Deville S (1993) Ice-templating, freeze-casting: beyond material processing. J Mater Res 28:2202–2219

Dragan ES (2014) Design and applications of interpenetrating polymer network hydrogels. A review. Chem Eng J 243:572–590. https://doi.org/10.1016/j.cej.2014.01.065

Eftekhari-Sis B, Rahimkhoei V, Akbari A, Araghi HY (2018) Cubic polyhedral oligomeric silsesquioxane nano-cross-linked hybrid hydrogels: synthesis, characterization, swelling and dye adsorption properties. React Funct Polym 128:47–57. https://doi.org/10.1016/j.reactfunctpolym.2018.05.00

Fekete T, Borsa J, Takács E et al (2014) Synthesis of cellulose derivative based superabsorbent hydrogels by radiation induced crosslinking. Cellulose 21:4157. https://doi.org/10.1007/s10570-014-0445-6

Foo KY, Hameed BH (2010) Insights into the modeling of adsorption isotherm systems. Chem Eng J 156:2–10. https://doi.org/10.1016/j.cej.2009.09.013

Giannouli P, Morris ER (2003) Cryogelation of xanthan. Food Hydrocolloids 17:495–501. https://doi.org/10.1016/S0268-005X(03)00019-5

Gibson LJ, Ashby MF (1997) Cellular solids: structure and properties, 2nd edn. Cambridge University Press, Cambridge

Heinze T, Koschella A (2005) Carboxymethyl ethers of cellulose and starch: a review. Macromol Symp 223:13–40. https://doi.org/10.1002/masy.200550502

Impert O, Katafias A, Kita P, Mills A, Pietkiewicz-Graczyk A, Wrzeszcz G (2003) Kinetics and mechanism of a fast leuco-methylene blue oxidation by copper(II)–halide species in acidic aqueous media. Dalton Trans 0:348–353. https://doi.org/10.1039/B205786G

Li Y, Shoemaker CF, Ma J, Shen X, Zhong F (2008) Paste viscosity of rice starches of different amylose content and carboxymethylcellulose formed by dry heating and the physical properties of their films. Food Chem 109:616–623. https://doi.org/10.1016/j.foodchem.2008.01.023

Lin Q, Gao M, Chang J, Ma H (2016) Adsorption properties of crosslinking carboxymethyl cellulose grafting dimethyldiallylammonium chloride for cationic and anionic dyes. Carbohydr Polym 151:283–294. https://doi.org/10.1016/j.carbpol.2016.05.064

Liu Y, Wang W, Wang A (2010) Adsorption of lead ions from aqueous solution by using carboxymethyl cellulose-g-poly (acrylic acid)/attapulgite hydrogel composites. Desalination 259:258–264. https://doi.org/10.1016/j.desal.2010.03.039

Marani PL, Bloisi GD, Petri DFS (2015) Hydroxypropylmethyl cellulose films crosslinked with citric acid for control release of nicotine. Cellulose 22:3907–3918

Mariano M, Hantao LW, Bernardes JS, Strauss M (2018) Microstructural characterization of nanocellulose foams prepared in the presence of cationic surfactants. Carbohydr Polym 195:153–162. https://doi.org/10.1016/j.carbpol.2018.04.075

Martins BF, Toledo PVO, Petri DFS (2017) Hydroxypropyl methylcellulose based aerogels: synthesis, characterization and application as adsorbents for wastewater pollutants. Carbohydr Polym 155:173–181. https://doi.org/10.1016/j.carbpol.2016.08.082

Ngah WSW, Fatinathan S (2008) Adsorption of Cu(II) ions in aqueous solution using chitosan beads, chitosan–GLA beads and chitosan–alginate beads. Chem Eng J 143:62–72. https://doi.org/10.1016/j.cej.2007.12.006

Roland CM (2013) Interpenetrating polymer networks (IPN): structure and mechanical behavior. In: Kobayashi S, Müllen K (eds) Encyclopedia of polymeric nanomaterials. Springer, Berlin. https://doi.org/10.1007/978-3-642-36199-9_91-1

Saber-Samandari S, Saber-Samandari S, Heydaripour S, Abdouss M (2016) Novel carboxymethyl cellulose based nanocomposite membrane: synthesis, characterization and application in water treatment. J Environ Manag 166:457–465. https://doi.org/10.1016/j.jenvman.2015.10.045

Scotti KL, Dunand DC (2018) Freeze casting: a review of processing, microstructure and properties via the open data

repository, FreezeCasting.net. Prog Mater Sci 94:243–305. https://doi.org/10.1016/j.pmatsci.2018.01.001

Seki Y, Altinisik A, Demircioğlu B, Tetik C (2014) Carboxymethylcellulose (CMC)–hydroxyethylcellulose (HEC) based hydrogels: synthesis and characterization. Cellulose 21:1689–1698. https://doi.org/10.1007/s10570-014-0204-8

Silverstein RM, Webster FX, Kiemle DJ, Bryce DL (2014) Spectrometric identification of organic compounds, 8th edn. Wiley, New York

Smirnova I, Gurikov P (2017) Aerogels in chemical engineering: strategies toward tailor-made aerogels. Annu Rev Chem Biomol Eng 8:1410–1428. https://doi.org/10.1146/annurev-chembioeng-060816-101458

Soares KV, Masini JC, Torresi RM, Carmona-Ribeiro AM, Petri DFS (2005) Hybrid particles of polystyrene and carboxymethyl cellulose as substrates for copper ions. Langmuir 21:8515–8519. https://doi.org/10.1021/la050493r

Souza IFT, Petri DFS (2018) β-Cyclodextrin hydroxypropyl methylcellulose hydrogels for bisphenol A adsorption. J Mol Liq 266:640–648. https://doi.org/10.1016/j.molliq.2018.06.117

Thielking H, Schmidt M (2012) Ullmann encyclopedia of industrial chemistry, vol 7. Wiley, Weinheim, pp 381–397

Tran HN, You SJ, Hosseini-Bandegharaei A, Chao HP (2017) Mistakes and inconsistencies regarding adsorption of contaminants from aqueous solutions: a critical review. Water Res 120:88–116. https://doi.org/10.1016/j.watres.2017.04.014

Vasić S, Grobéty B, Kuebler J, Graule T, Baumgartner L (2007) X-ray computed micro tomography as complementary method for the characterization of activated porous ceramic preforms. J Mater Res 22:1414–1424. https://doi.org/10.1557/jmr.2007.0181

Wang W, Wang Q, Wang A (2011) PH-responsive carboxymethylcellulose-g poly (sodium acrylate)/poly(vinylpyrrolydone) semi-IPN hydrogels withenhanced responsive and swelling properties. Macromol Res 19:57–65. https://doi.org/10.1007/s13233-011-0112-9

Weber JW, Morris JC (1963) Kinetics of adsorption of carbon from solution. J Sanit Eng Div Am Soc Civ Eng 89:31–39

Yang S, Fu S, Liu H, Zhou Y, Li X (2010) Hydrogel beads based on carboxymethyl cellulose for removal heavy metal ions. J Appl Polym Sci 119:1204–1210. https://doi.org/10.1002/app.32822

Zirak M, Abdollahiyan A, Eftekhari-Sis B, Saraei M (2017) Carboxymethyl cellulose coated $Fe_3O_4@SiO_2$ core–shell magnetic nanoparticles for methylene blue removal: equilibrium, kinetic, and thermodynamic studies. Cellulose 25:503–515. https://doi.org/10.1007/s10570-017-1590-5

Publisher's Note Springer Nature remains neutral with regard to jurisdictional claims in published maps and institutional affiliations.